Harmonic boundary conditions for circular inclusions and their coupling to external circuits

H.De Gersem and K.Hameyer

Abstract: The effect of the magnetic field in a homogeneous subdomain of a finite-element model is simulated by an analytical expression imposed at its boundary. In the case of a stranded or a solid conductor cross-section, the coupling to an external circuit is considered. The hybrid finite-element harmonic-boundary equivalent-circuit approach offers the designer a powerful simulation tool, yielding models attaining the same accuracy when compared to pure finite-element models but requiring less (by a factor of 10) computation time. The relationships with the boundary-element method and impedance boundary conditions are established. The application of the methods proposed for a cable model illustrates the benefits of the proposed approach.

1 Introduction

Quasi-static electromagnetic simulation of technical devices suffers from difficulties related to the nonlinear characteristics of ferromagnetic materials, the complicated geometries, the sophisticated excitation patterns and the need to consider second-order effects such as expansion due to heating and mechanical deformation [1, 2]. Hence, modelling, e.g. transferring a device into a discrete model fitting within the available computational resources, tends to become a designing process in itself. Finite-element (FE) simulation is widespread, mainly because of its natural suitability to consider arbitrary geometries and nonlinearities at a local level. For certain parts of a model, e.g. airgaps, cooling ducts, small conductors, far-field regions and sliding surfaces, other discretisation methods, such as the boundary-element (BE) method (BEM), equivalent circuit (EC) simulation and local analytical solutions, may be more convenient. The combination of two or more discretisation methods within the same model, yields hybrid approaches, e.g. FEM–BEM [3] and FEM–EC [4]. For a large range of models, the application of analytical solutions to parts of the model is advantageous. In this paper, local analytical approaches for circular inclusions in 2-D magnetic models are presented. The emphasis is put on their formulation as boundary conditions, here called 'harmonic boundary conditions' (HBC), and their application to conductors embedded in external electric circuits. Technical examples illustrate the flexibility and the benefits of the presented approach.

© IEE, 2001

IEE Proceedings online no. 20010532

DOI: 10.1049/ip-smt:20010532

Paper first received 10th November 2000 and in revised form 14th May 2001

H. De Gersem was with the Katholieke Universiteit Leuven, Dep. ESAT, Div. ELEN, and is now with the Computational Electromagnetics Laboratory, Darmstadt University of Technology, Schloßgartenstraße 8, D-64289 Darmstadt, Germany

K. Hameyer is with the Katholieke Universiteit Leuven, Dep. ESAT, Div. ELEN, Kasteelpark Arenberg 10, B-3001 Leuven-Heverlee, Belgium

2 Local analytical models

Consider a two-dimensional (2-D) model with the computational domain $\Omega_f \cup \Omega_s$ consisting of the subdomaln Ω_f, discretised by FEs and the subdomain Ω_s to which analytical models are applied (Fig. 1*a*). Suppose the boundary Γ_s of the subdomain Ω_s consisting of a finite set of simple primitives and the materials within Ω_s homogeneous, linear and isotropic. The magnetic field within Ω_s is described by a second-order partial differential equation (PDE). If the field quantities at Γ_s are known, an analytical solution for the magnetic field inside Ω_s can be constructed. Hence, the accuracy of the simulation results within Ω_s only depends on the accuracy of the material data, the boundary conditions and the excitation.

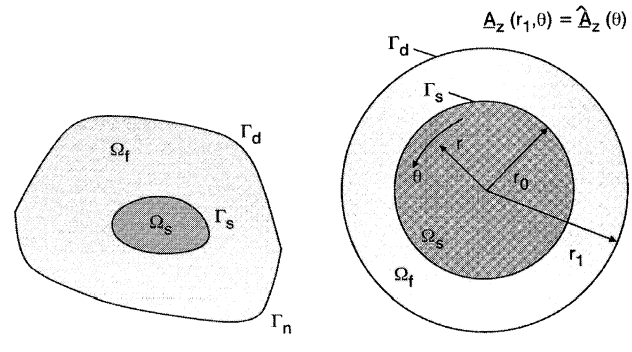

Fig. 1 *Computational domain $\Omega_f \cup \Omega_s$ and the benchmark solid conductor model*

Numerical methods for solving PDEs approximate the exact solution by a series expansion in terms of a finite set of base functions, e.g. FEs and BEs defined upon a mesh, currents and voltages defined along EC branches. If the space spanned by the base functions is not eligible to reflect the true behaviour of the considered field, the approximation will be poor. In subregions of the model in which an analytical solution exists, this can be overcome by plugging the local analytic expression for the magnetic field into the FE model. This local intervention may substantially enhance the accuracy of the overall computation.

In general, an analytical solution is constructed as an infinite series expansion of the eigenfunctions of the differential operator. For particular shapes of Ω_s these eigenfunctions simplify to very easy expressions, e.g. a Fourier series developed at the circular border of a disc (Fig. 1*b*). The analytical solution is expressed in terms of the still unknown field quantities at the boundary. Its derivative relates the flux and the magnetomotive force at each point of Γ_s to each other. The expression is plugged into the FE formulation as a boundary condition.

Local 2-D and 3-D analytical solutions in combination with FE methods are already proposed as highly accurate post-processing tools in [5, 6]. Here, the local analytical solution is embedded in the solution process of the FE model itself. All approaches aim at enhancing the accuracy or reducing the model size by partially relying on analytical techniques.

3 Finite-element formulation

By the choice of the magnetic vector potential $\boldsymbol{A}$ by $\boldsymbol{B} = \nabla \times \boldsymbol{A}$, the magnetic flux density $\boldsymbol{B}$ is assumed to be divergence-free. The integration of Faraday-Lenz's law yields $\boldsymbol{E} = -\nabla V - \partial \boldsymbol{A}/\partial t$ with $\boldsymbol{E}$ the electric field and V the electric scalar potential. The formulation applied here is the $\boldsymbol{A} - V$ formulation expressing Ampère's law by

$$\nabla \times (\nu \nabla \times \boldsymbol{A}) + \sigma \frac{\partial \boldsymbol{A}}{\partial t} = -\sigma \nabla V \tag{1}$$

ν and σ are the reluctivity and the conductivity of the material. $\mu = 1/\nu$ is the permeability. For 2-D models with a translatory symmetry and a voltage drop ∇V only in the z-direction, eqn. 1 simplifies to

$$-\nabla \cdot (\nu \nabla A_z) + \sigma \frac{\partial A_z}{\partial t} = -\frac{\sigma}{\ell_z} \Delta V \tag{2}$$

with A_z the z-component of $\boldsymbol{A}$ and ℓ_z the length of the model. In this paper, only time-harmonic excitation is considered. The methods presented here, however, easily generalise to transient, axisymmetric and 3-D models. All material parameters are assumed to be constant in time. Nonlinearities are resolved by successive approximations based on effective material characteristics [7]. The field quantities are represented by their respective phasors:

$$A_z(t) = \mathrm{Re}\left\{\underline{A}_z \mathrm{e}^{\jmath \omega t}\right\} \tag{3}$$

$$\Delta V(t) = \mathrm{Re}\left\{\Delta \underline{V} \mathrm{e}^{\jmath \omega t}\right\} \tag{4}$$

with $\omega = 2\pi f$ the pulsation and f the frequency of the applied excitation. The governing PDE is

$$-\nabla \cdot (\nu \nabla \underline{A}_z) + \jmath \omega \sigma \underline{A}_z = -\frac{\sigma}{\ell_z} \Delta \underline{V} \tag{5}$$

The magnetic vector potential is discretised on Ω_f by n_f base functions $N_j(x, y)$ with as supports, the sets of triangular elements surrounding each of the mesh vertices:

$$\underline{A}_z = \sum_{j=1}^{n_f} \underline{A}_{zj} N_j(x, y) \tag{6}$$

The Galerkin FE method consists of weighting eqn. 5 by the same functions N_i along Ω_f. The resulting symmetric system of equations is

$$\sum_j^{n_f} (k_{ij} + l_{ij}) \underline{A}_{zj} + g_i = f_i, \quad i = 1, \ldots, n_f \tag{7}$$

with

$$k_{ij} = \int_{\Omega_f} \nu \nabla N_i \cdot \nabla N_j \mathrm{d}\Omega \tag{8}$$

$$l_{ij} = \int_{\Omega_f} \jmath \omega \sigma N_i N_j \mathrm{d}\Omega \tag{9}$$

$$g_i = -\int_{\Gamma} \nu \frac{\partial \underline{A}_z}{\partial n} N_i \mathrm{d}\Gamma \tag{10}$$

$$f_i = \int_{\Omega_f} \frac{\sigma}{\ell_z} \Delta \underline{V} N_i \mathrm{d}\Omega \tag{11}$$

with $\partial/\partial n$ the normal derivative outward to Γ. The partitions of $\Gamma = \Gamma_d \cup \Gamma_n \cup \Gamma s$ correspond to the following.

Γ_d: *Dirichlet boundary condition*: Γ_d is a flux wall. The magnetic vector potential is constrained to a prescribed value. There are no FE shape functions associated with the nodes on Γ_d. Hence, the coefficients k_{ij}, l_{ij}, g_i and f_i for all nodes i on Γ_d vanish.

Γ_n: *Homogeneous Neumann boundary condition*: Γ_n is a flux gate, $\partial A_z/\partial n = 0$ and g_i for all i on Γ_n vanishes.

Γ_s: *Robbins boundary condition*: For second-order PDEs, a Robbins boundary condition brings the field quantity into relation with its normal derivative. This represents the relation between the flux and the magnetomotive force at Γ_s. Ω_s behaves somehow like a black-box magnetic impedance experienced by the magnetic field of Ω_f. This expression is inserted in g_i.

4 Analytical circular inclusion

Consider the disc Ω_s with radius r_0 of Fig. 1*b*. The reluctivity ν and the conductivity σ are assumed to be homogeneous and linear. The governing PDE eqn. 5 within Ω_s is in cylindrical coordinates (r, θ):

$$-\frac{1}{r}\frac{\partial}{\partial r}\left(\nu r \frac{\partial \underline{A}_z}{\partial r}\right) - \frac{1}{r^2}\frac{\partial}{\partial \theta}\left(\nu \frac{\partial \underline{A}_z}{\partial \theta}\right) + \jmath \omega \sigma \underline{A}_z = \frac{\sigma}{\ell_z} \Delta \underline{V} \tag{12}$$

The first two terms are diffusive, the third is a reaction term modelling the eddy currents, the one on the right-hand side represents the electrical excitation. The voltage drop phasor $\Delta \underline{V}$ only depends on r. By separation of variables, the analytical solution for this particular geometry is

$$\underline{A}_z(r, \theta) = S(r) + \underline{a}_0 R_0(r) + \sum_{k=1}^{\infty} R_k(r)\left(\underline{a}_k \cos(k\theta) + \underline{b}_k \sin(k\theta)\right) \tag{13}$$

$S(r)$, here called the excitation function, is the particular solution of the nonhomogeneous PDE with $S(r_0) = 0$. The other terms constitute the solution of the homogeneous PDE. The impedance functions $R_k(r)$ depend upon the presence of the reaction term. The FE approximation at Γ_s determines the Fourier coefficients of $\underline{A}_z$ at Γ_s:

$$\underline{a}_0 = \sum_{j=1}^{n_s} \underline{A}_{zj} \frac{1}{2\pi} \underbrace{\int_0^{2\pi} N_j(r_0, \theta) \mathrm{d}\theta}_{u_{j0}} \tag{14}$$

$$\underline{a}_k = \sum_{j=1}^{n_s} \underline{A}_{zj} \frac{1}{\pi} \underbrace{\int_0^{2\pi} N_j(r_0, \theta) \cos(k\theta) \mathrm{d}\theta}_{u_{jk}} \tag{15}$$

$$\underline{b}_k = \sum_{j=1}^{n_s} \underline{A}_{zj} \frac{1}{\pi} \underbrace{\int_0^{2\pi} N_j(r_0, \theta) \sin(k\theta) \mathrm{d}\theta}_{v_{jk}} \tag{16}$$

n_s is the number of nodes on Γ_s. From here on, i and j count the nodes on Γ_s, and N_i and N_j denote the FE shape

functions restricted to Γ_s. The diffusion through Γ_s is

$$g_i = \int_0^{2\pi} \nu \frac{\partial \underline{A}_z}{\partial r}(r_0, \theta) N_i r_0 \mathrm{d}\theta \tag{17}$$

and, in general, depends on the magnetic vector potentials $\underline{A}_{jz}$ at Γ_s,

$$g_i = h_i + \sum_{j=1}^{n_s} (m_{ij} + d_{ij}) \underline{A}_{zj} \tag{18}$$

by the boundary diffusion coefficients

$$h_i = \nu r_0 S'(r_0) u_{i0} \tag{19}$$

$$m_{ij} = \frac{\nu}{2\pi} r_0 R_0'(r_0) u_{i0} u_{j0} \tag{20}$$

$$d_{ij} = \sum_{k=1}^{\infty} \frac{\nu}{\pi} r_0 R_k'(r_0)(u_{ik}u_{jk} + v_{ik}v_{jk}) \tag{21}$$

The coefficients m_{ij} and d_{ij} are added to the coefficient matrix, the terms h_i to the right-hand side. $m_{ij} = m_{ji}$, $d_{ij} = d_{ji}$ and hence the symmetry of the system matrix is preserved. As $d_{ij} \neq 0$ for all nodes i and j on Γ_s, a relatively dense part is introduced in the system matrix. In the following Sections, dealing with particular kinds of circular inclusion, the impedance and excitation functions are defined.

5 Nonconductive inclusion

For nonconductive circular inclusions, e.g. cooling channels, eqn. 12 simplifies to the Laplace equation. The excitation and impedance impedance functions are

$$S(r) = 0 \tag{22}$$

$$R_k(r) = \left(\frac{r}{r_0}\right)^k \tag{23}$$

The boundary diffusion coefficients are

$$h_i = 0 \tag{24}$$

$$m_{ij} = 0 \tag{25}$$

$$d_{ij} = \sum_{k=1}^{\infty} \frac{\nu}{\pi} k(u_{ik}u_{jk} + v_{ik}v_{jk}) \tag{26}$$

m_{ij} vanishes, indicating the independence of the Laplacian on a constant term.

6 Stranded conductor

Consider a stranded conductor with current I_{str}, N_{str} turns, the circular cross-section Ω_{str} with surface $\Delta_{str} = \pi {r_0}^2$ and boundary Γ_{str} (Fig. 2*a*). The fill factor f_{str} denotes the fraction of conductive material in Ω_{str} The current density in Ω_{str} is assumed to be constant and replaces the source term in eqn. 12.

$$J_{str} = \frac{N_{str}}{\Delta_{str}} I_{str} \tag{27}$$

The lack of eddy currents is imposed by omitting the reaction term in eqn. 12. Hence, the differential operator and the impedance functions remain the same as in the previous case. The source term gives rise to the excitation term

$$S_{str}(r) = -\frac{\mu(r^2 - r_0^2)}{4} J_{str} \tag{28}$$

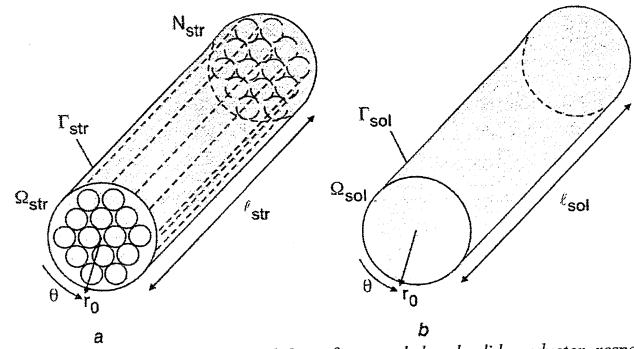

Fig. 2 *Cross-sections Ω_{str} and Ω_{sol} of a stranded and solid conductor, respectively, modelled by a HBC within an FE model*
a Stranded conductor
b Solid conductor

Hence, the weak form g_i at Γ_{str} only differs in the term

$$h_i = -\frac{N_{str}}{2\pi} u_{i0} I_{str} = p_{i,str} I_{str} \tag{29}$$

reflecting the magnetomotive force excited by the stranded conductor experienced by the flux crossing Γ_s. In the case of current excitation, this term is put on the right-hand side. If the stranded conductor is embedded in a more sophisticated electrical circuit, I_{str} is treated as an unknown and the terms in eqn. 29 remain on the left-hand side. An extra equation is required to describe the electrical behaviour of the stranded conductor. The voltage drop ΔV_{str} across the stranded conductor is expressed in terms of the average voltage drop experienced by the wires:

$$\Delta V_{str} = \frac{N_{str}\ell_{str}}{\Delta_{str}} \int_{\Omega_{str}} (-\nabla V(x,y)) \mathrm{d}\Omega \tag{30}$$

Stranded conductors prevent eddy currents and the corresponding losses. They, however, experience induced voltages. Because of Faraday–Lenz's law, the gradient of the electric scalar potential is related to the current and the magnetic field by

$$-\nabla V = \frac{J_{str}}{f_{str}\sigma} + \jmath\omega \underline{A}_z(x,y) \tag{31}$$

Hence, the voltage drop across a stranded conductor is

$$\Delta V_{str} = (R_{str} + \jmath\omega L_{str}) I_{str} + \sum_{j=1}^{n_s} \underline{A}_{zj} \jmath\omega \ell_{str} \frac{N_{str}}{2\pi} u_{j0} \tag{32}$$

$$R_{str} = \frac{N_{str}^2 \ell_{str}}{f_{str}\sigma\Delta_{str}} \tag{33}$$

$$L_{str} = \frac{\mu N_{str}^2 \ell_{str}}{8\pi} \tag{34}$$

R_{str} is the DC-resistance of the stranded conductor. The self-inductance L_{str} corresponds to the situation where no flux crosses Γ_{str} and the inductor only experiences the flux excited by itself. Eqn. 32 is scaled by the factor $-\chi_{str} = -1/\jmath\omega\ell_{str}$ in order to symmetrise it with respect to the respective terms of eqn. 29 in the magnetic equations.

7 Solid conductor

In the case of a solid conductor, a reaction term appears in the PDE. The analytical solution is much more complicated when compared to the previous cases. The excitation and impedance functions are

$$S_{sol}(r) = \frac{\Delta V_{sol}}{\jmath\omega\ell_{sol}} \left(1 - \frac{I_0(\xi r)}{I_0(\xi r_0)}\right) \tag{35}$$

$$R_{sol,k}(r) = \frac{I_k(\xi r)}{I_k(\xi r_0)} \tag{36}$$

with ℓ_{sol} the length and ΔV_{sol} the voltage drop along the solid conductor (Fig. 2*b*). I_k denotes the modified Bessel function of the first kind of order k and $\xi = \sqrt{(\jmath\omega\sigma\mu)}$. The additional terms in the system of equations are

$$h_i = -\frac{\nu}{\jmath\omega\ell_{sol}} \frac{\xi r_0 I_1(\xi r_0)}{I_0(\xi r_0)} u_{i0}\Delta V_{sol} = q_{i,sol}\Delta V_{sol} \tag{37}$$

$$m_{ij} = \frac{\nu}{2\pi} \frac{\xi r_0 I_0'(\xi r_0)}{I_0(\xi r_0)} u_{i0}u_{j0} \tag{38}$$

$$d_{ij} = \sum_{k=1}^{\infty} \frac{\nu}{\pi} \frac{\xi r_0 I_k'(\xi r_0)}{I_k(\xi r_0)} (u_{ik}u_{jk} + v_{ik}v_{jk}) \tag{39}$$

Similar to the stranded conductor case, ΔV_{sol} may be unknown. An additional equation for the total current I_{sol} through the solid conductor is appended to the system:

$$I_{sol} = \int_{\Omega_{sol}} J_{sol} \mathrm{d}\Omega = Y_{sol}\Delta V_{sol} - \sum_{j=1}^{n_s} \chi q_{j,sol}\underline{A}_{zj} \tag{40}$$

$$Y_{sol} = \frac{\sigma\pi r_0^2}{\ell_{sol}} \frac{2}{\xi r_0} \frac{I_1(\xi r_0)}{I_0(\xi r_0)} \tag{41}$$

Y_{sol} is the AC admittance of the solid conductor when isolated from the rest of the model. The limit of Y_{sol} for $\omega \to 0$ yields the DC conductance of the solid conductor. The additional circuit equation is symmetrised with respect to the unknown excitation term eqn. 35 by the factor $\chi_{sol} = 1/\jmath\omega\ell_{sol}$.

8 External circuit coupling

The solid and stranded conductors in the magnetic model are embedded within an external lumped parameter model, comprising external voltage and current sources, resistors, inductors and capacitors. The expressions in eqns. 32 and 40 fit within the topological field-circuit coupling scheme developed in Fig. 8. The method yields a few extra equations in the coupled system matrix while preserving the symmetry of the system.

9 Implementation issues

In practice, the application of an infinite series at Γ_s is impossible. Moreover, it is not recommended as in most models, only a few terms are already sufficient to ensure an accuracy far beyond the one provided by the FE discretisation. All Fourier series considered in the practical computations are truncated to k_{max} terms. An adaptive choice of k_{max} is suggested by the Nyquist criterion relating the number of harmonics treated by the HBC, to the number of FE nodes on Γ_s. In the case of solid conductors, the Bessel functions have to be evaluated with an appropriate accuracy. For large orders, this may become especially troublesome. All expressions containing Bessel functions are rewritten in a form suited for numerical calculus, and specialised routines have been applied [9–11].

10 Discretisation error

The convergence of the discretisation error is studied by a numerical experiment. A solid conductor model for which an analytical solution exists, serves as a benchmark to compare the coupled FEM–HBC approach to conventional FE simulation (Fig. 1*b*). The copper solid conductor is surrounded by air and submitted to a homogeneous magnetic field pulsating at 500 Hz. The choice of the geometrical dimensions is guided by the typical situation in wire windings where the cross-sections of the conductors only constitute a fraction of the cross-section of the entire winding. As an error indication, the computed power loss is referred to the analytically obtained results. The convergence of the error with respect to the number of degrees of freedom is plotted in Fig. 3. As HBC does not need a mesh within the solid conductor cross-section, it is obvious that this approach attains a prescribed accuracy for smaller models when compared to pure FEM. This is however an unfair comparison, because the FEM–HBC formulation yields a more dense matrix and, hence, requires relatively more time to solve the system of equations by iterative solvers. Fig. 4 indicates however that also with respect to the computation time, FEM–HBC outperforms conventional FEM. As in this benchmark model only one spatial harmonic is present in the excitation, the series expansion constructed by the HBC boundary condition already attains an optimal Fourier expansion for $k_{max} = 1$. As a

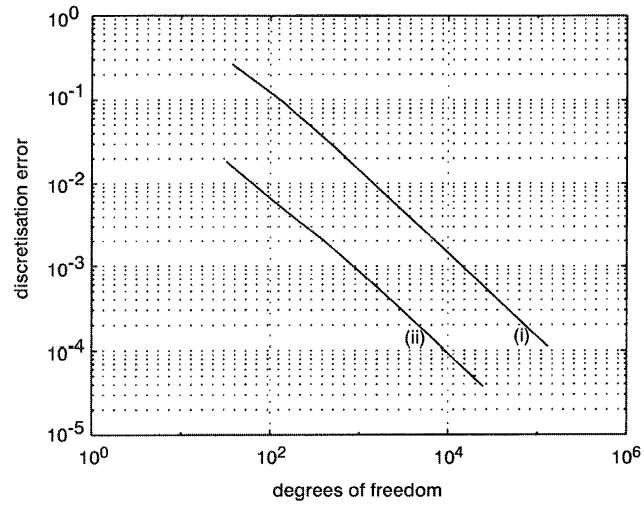

Fig. 3 *Convergence of FEM and FEM–HBC discretisation errors with respect to number of degrees of freedom for a HBC in a homogeneous field*
(i) FEM
(ii) FEM–HBC

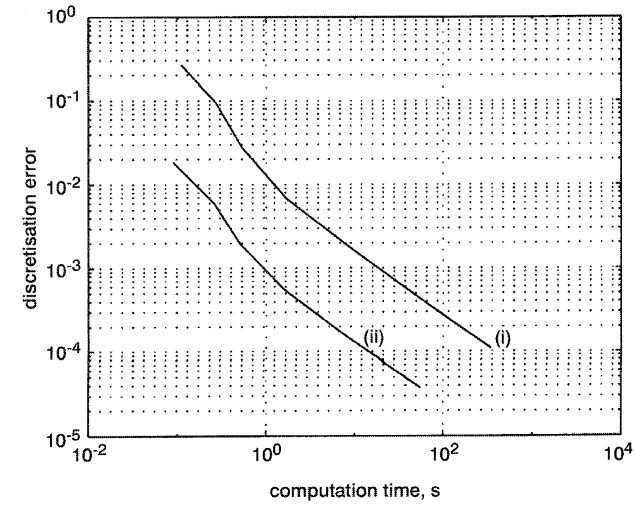

Fig. 4 *Convergence of FEM and FEM–HBC discretisation errors with respect to computation time for a HBC in a homogeneous field*
(i) FEM
(ii) FEM–HBC

consequence, this particular boundary condition favours the HBC treatment and the benchmark still lacks generality. In Fig. 5, the convergence study is repeated for an excitation of the form

$$\underline{A}_z(r_1,\theta) = \begin{cases} -\underline{\hat{a}} r_0 & \text{if } x < -r_0 \\ \underline{\hat{a}} x & \text{if } -r_0 < x < r_0 \\ \underline{\hat{a}} r_0 & \text{if } x > r_0 \end{cases} \quad (42)$$

Now, an infinite set of spatial harmonics is present in the excitation and hence in the field solution. The influence of k_{max} on the accuracy is considered in Fig. 5. The numerical experiment indicates that the accuracy depends more on n_s than on k_{max}. Also, doubling k_{max} only increases the computation time by a few percent, whereas doubling the number of FE nodes multiplies the latter by a factor of 3. The observed convergence behaviour motivates the application of the FEM–HBC approach to technical models incorporating regularly shaped, linear and homogeneous inclusions.

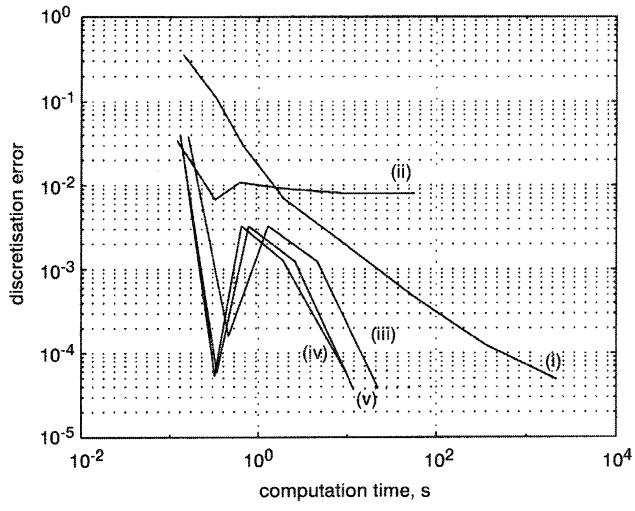

Fig. 5 *Convergence of FEM and HBC–FEM discretisation errors with respect to computation time for a HBC in an arbitrary field*
(i) FEM
(ii)–(v) FEM–HBC for k_{max} 1, 4, 16, 64

11 Relation to BEM

Both, BEM and HBC only consider discretisations on the boundary of the subdomain of interest. This suggests a strong relationship between BEM and HBC. There are, however two important differences: discretisation and shape.

Discretisation; BEM approximates the exact solution by a series expansion of local Green's functions, whereas HBC applies harmonic functions. As the latter are eigenfunctions of the PDE, the solution at the boundary is exactly propagated towards the inside of Ω_s. At the boundary, the convergence of the piecewise polynomial approximation applied by BEM is governed by the properties of the Taylor expansion, the order of polynomials and the mesh size. Fourier series feature uniform convergence which may be more accurate.

Shape: BEM is applicable to subdomains with arbitrary geometries, whereas a HBC requires an analytical solution to be developed for each particular shape of the domain. As a consequence, HBC does not offer the same general applicability as BEM.

The implementation of HBC is only recommended for some particular geometries that frequently occur in the technical models considered, e.g. cooling channels, solid and stranded conductor with circular cross-sections in electromagnetic devices. HBC is only beneficial when combined with a general discretisation method and, in the case of conductors, also coupled to a circuit description. Here, HBC coupled to FEM and ECs, is presented as an enrichment of the set of available modelling tools, enabling fast and accurate simulation of complicated models that may be unsolvable by conventional approaches used so far. A similar inclusion of an analytical model has been considered for the airgap of electrical machines in [2, 12].

12 Relation to impedance boundary conditions

A magnetic shield for which the geometrical dimensions exceed the experienced skin depth, is almost impervious for magnetic flux. An impedance boundary condition (IBC) is an efficient modelling technique relating the electric and magnetic fields at the material interfaces to each other [13]. Also with respect to IBCs, external circuit connections can be considered [14]. The fine discretisation of the thin current layer at the shield surface is avoided. More generally, an IBC is a small parameter problem, i.e. treating one of the characteristic lengths, e.g. the skin depth or the region's thichness, as negligible when compared to other dimensions [15]. The subdomain is replaced by a boundary condition at its border. HBCs do not rely on these limit assumptions. HBCs model the true geometry and excitation. The difference in characteristic length is not essential, nor is it prohibitive. In fact, HBCs become advantageous over FEs for modelling small skin depths, e.g. in solid conductors operated at elevated frequencies.

13 Application: cable

A cable (part of a low-voltage power grid) experiences, besides the 50 Hz component, a considerable amount of harmonic distortion. The cable consists of 35 wires connected in parallel and is surrounded by insulation material, a cage preventing the outside magnetic field and a shell for mechanical protection (Fig. 6). Owing to skin and proximity effects and due to the magnetic shielding of the cable, its response strongly depends on the applied frequency. The FE simulation of this model is cumbersome, because the meshing of the thin current layers corresponding to elevated frequencies becomes insurmountable. Here, instead, HBCs have been applied to the individual wires (Fig. 7). The HBC formulation achieves highly accurate results, even if a skin depth of only a few micrometres is involved (Fig. 8). The twisting of the cable wires is considered by an external circuit connecting all wires in series. The dependence of the voltage drop on the applied frequency is simulated by the FEM–HBC–EC method (Fig. 9).

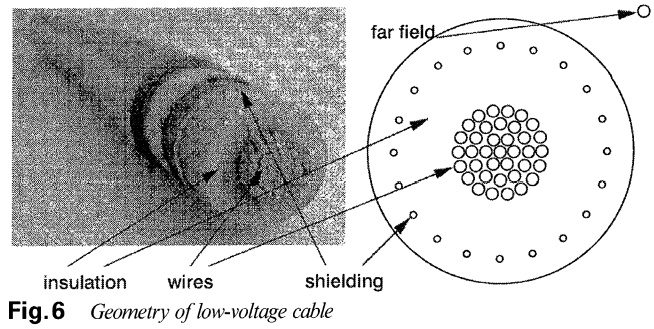

Fig. 6 *Geometry of low-voltage cable*

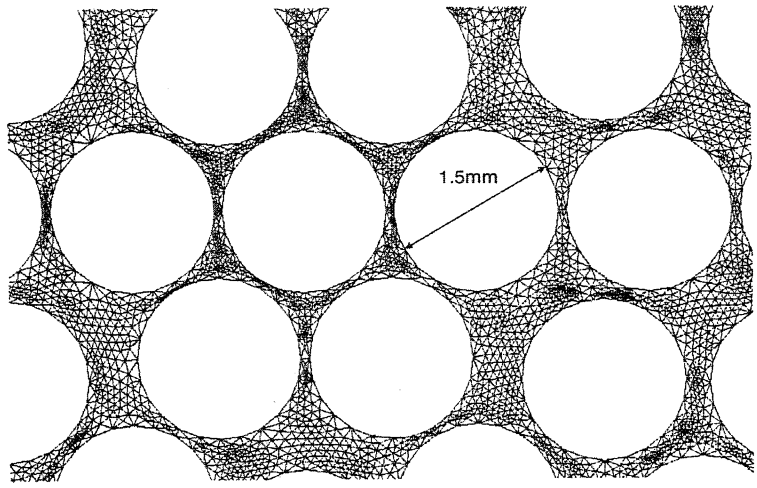

Fig. 7 *Detail of FE mesh with HBCs of cable model*

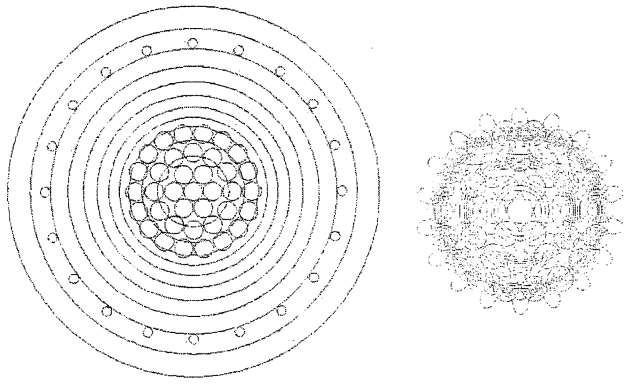

Fig. 8 *Magnetic flux plot of cable model at two instants of time*
a When the current attains its maximum
b One quarter of a period later

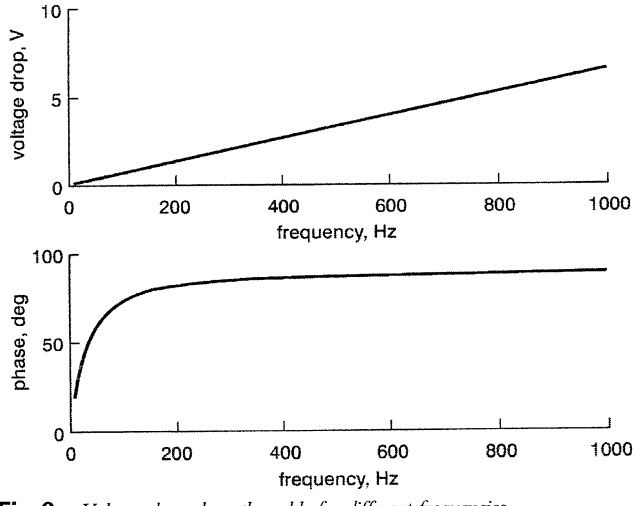

Fig. 9 *Voltage drop along the cable for different frequencies*

14 Conclusions

HBCs have been applied to conductors within an FE model, to avoid meshing problems related to small skin depth. A HBC–EC coupling scheme has been developed. The hybrid FEM–HBC–EC approach was shown to offer the same modelling flexibility and accuracy as the FEM, with models which are by a factor of 10 smaller. This has been illustrated by a cable model.

15 Acknowledgments

The authors are grateful to the Belgian 'Fonds voor Wetenschappelijk Onderzoek Vlaanderen' (G.0427.98) and the Belgian Ministry of Scientific Research (IUAP No. P4/20) for the financial support of this work.

16 References

1 HAMEYER, K., and BELMANS R.: 'Numerical modelling and design of electrical machines and devices' (WIT Press, Southampton, UK, 1999)
2 SALON, S.J.: 'Finite element analysis of electrical machines' (Kluwer Academic Publishers, Boston, 1995)
3 KURZ, S., FETZER, J., and LEHNER, G.: 'Threedimensional transient BEM-FEM coupled analysis of electrodynamic levitation problems', *IEEE Trans. Magn.*, 1996, **32**, (3), pp. 1062–1065
4 KANERVA, S.: 'Circuit simulator in coupled field-circuit problems'. Proceedings of the international conference on *Electrical Machines (ICEM00)*, Helsinki, Finland, August 2000, Vol. 1, pp. 501–504
5 KASPER, M., and FRANZ, J.: 'Highly accurate computation of field quantities and forces by superconvergence in finite-elements', *IEEE Trans. Magn.*, 1995, **31**, (3), pp. 1424–1427
6 HAMEYER, K., MERTENS, R., PAHNER, U., and BELMANS, R.: 'New technique to enhance the accuracy of 2-d/3-d field quantities and forces obtained by standard finite-element solutions', *IEE Proc. Sci., Meas. Technol.*, 1998, **145**, (2), pp. 67–75
7 LEDERER, D., IGARASHI, H., and KOST, A.: 'Modelling of nonlinear magnetic material using an effective permeability - comparison between different formulations', *Appl. Comput. Electromagn. Soc. J.*, 1997, **12**, pp. 113–116
8 DE GERSEM, H., MERTENS, R., PAHNER, U., BELMANS, R., and HAMEYER, K.: 'A topological method used for field-circuit coupling', *IEEE Trans. Magn.*, 1998, **34**, (5), pp. 3190–3193
9 WATSON, G.N.: 'A treatise on the theory of Bessel functions' (Cambridge University Press, Cambridge, 1966, 2nd edn.)
10 ABRAMOWITZ, M., and STEGUN, I.A.: 'Handbook of mathematical functions' (Dover Publications, New York, 1965)
11 AMOS, D.E.: 'A portable package for Bessel functions of a complex argument and nonnegative order', *ACM Trans. Math. Softw.*, 1986, **12**, (3), pp. 265–273
12 LEE, K.S., DEBORTOLI, M.J., LEE, M.J., and SALON, S.J.: 'Coupling finite-elements and analytical solution in the airgap of electrical machines', *IEEE Trans. Magn.*, 1991, **27**, (5), pp. 3955–3957
13 YUFEREV, S., and IDA, N.: 'Selection of the surface impedance boundary conditions for a given problem', *IEEE Trans. Magn.*, 1999, **35**, (3), pp. 1486–1489
14 GYIMESI, M., and LAVERS, D.: 'Impedance boundary condition for multiply connected domains with exterior circuit conditions', *IEEE Trans. Magn.*, 1994, **30**, (5), pp. 3056–3059
15 BOSSAVIT, A.: 'Small parameter problems in eddy-current theory: a review, and a case-study on how to avoid meshing small air-gaps', *IEEE Trans. Magn.*, 1996, **32**, (3), pp. 729–732